SciencePG
Science Publishing Group

http://www.sciencepublishinggroup.com/j/wros
ISSN: 2328-7969
Volume 8 Number 3 June 2019

Journal of Water Resources and Ocean Science

Science Publishing Group, USA

Journal of Water Resources and Ocean Science

ISSN: 2328-7969 (PRINT) ISSN: 2328-7993 (ONLINE)

http://www.sciencepublishinggroup.com/j/wros

Journal of Water Resources and Ocean Science, **2019, 8(3), 28–43**
Published by Science Publishing Group online at http://www.sciencepublishinggroup.com/j/wros

CONTENTS

Vol. 8 No. 3 **June 2019**

Journal of Water Resources and Ocean Science (WROS)

JOURNAL INFORMATION

Journal of Water Resources and Ocean Science (WROS) is published bimonthly by Science Publishing Group (SciencePG), online at http://www.sciencepublishinggroup.com/j/wros

SUBMISSION

To submit, please visit: http://www.sciencepublishinggroup.com/login
Any questions, just contact: journal@sciencepublishinggroup.com

REPRINTS

Reprints of the published journal are issued by SciencePG.
Cost: 100USD/one hard copy.
E-mail: journal@sciencepublishinggroup.com

ADVANTAGES

Peer Review
All papers submitted to journals in SciencePG are peer-reviewed.

Fast Publication
Papers of good quality can be published within two months after being submitted to SciencePG.

High Visibility
Each journal in SciencePG uses the OpenURL standard, making it easy for libraries to link users as directly as possible from citation to the full text of the article.

Open Access
Open Access makes knowledge available to all, without the barrier of affordability and without restrictions on using it to develop related areas of research.

Abstracting and Indexing
WorldCat, CrossRef, JournalSeek, Academickeys, ResearchBib, Directory of Research Journals Indexing (DRJI) and others.

COPYRIGHT

For more information contact us by
E-mail: service@sciencepublishinggroup.com

Journal of Water Resources and Ocean Science
2019; 8(3): 28-36
http://www.sciencepublishinggroup.com/j/wros
doi: 10.11648/j.wros.20190803.11
ISSN: 2328-7969 (Print); ISSN: 2328-7993 (Online)

Models for Estimating Precipitable Water Vapour and Variation of Dew Point Temperature with Other Parameters at Owerri, South Eastern, Nigeria

Davidson Odafe Akpootu[1, *], Mukhtar Isah Iliyasu[2], Wahidat Mustapha[3], Simeon Imaben Salifu[4], Hassan Taiwo Sulu[2], Samson Philip Arewa[1], Mohammed Bello Abubakar[2]

[1]Department of Physics, Usmanu Danfodiyo University, Sokoto, Nigeria

[2]Physics Unit, Umaru Ali Shinkafi Polytechnic, Sokoto, Nigeria

[3]Nigerian Meteorological Agency (NIMET), Abuja, Nigeria

[4]Department of Physics, Kogi State College of Education Technical, Kabba, Nigeria

Email address:

davidson.odafe@udusok.edu.ng (D. O. Akpootu), profdon03@yahoo.com (D. O. Akpootu)

[*]Corresponding author

To cite this article:

Davidson Odafe Akpootu, Mukhtar Isah Iliyasu, Wahidat Mustapha, Simeon Imaben Salifu, Hassan Taiwo Sulu, Samson Philip Arewa, Mohammed Bello Abubakar. Models for Estimating Precipitable Water Vapour and Variation of Dew Point Temperature with Other Parameters at Owerri, South Eastern, Nigeria. *Journal of Water Resources and Ocean Science*. Vol. 8, No. 3, 2019, pp. 28-36. doi: 10.11648/j.wros.20190803.11

Received: August 26, 2019; **Accepted**: September 16, 2019; **Published**: October 9, 2019

Abstract: Precipitable water vapour (PWV) is a vital component of the atmosphere and appreciably controls many atmospheric processes. The PWV is not easy to measure with sufficient spatial and time resolution under all weather conditions. In this paper, three precipitable water vapour models; the Smith, Won and Leckner's models were evaluated and compared for Owerri (Latitude 5.48°N, Longitude 7.00°E, and 91 m above sea level) using meteorological parameters of monthly average daily maximum temperature, minimum temperature and relative humidity during the period of sixteen years (2000-2015). The Leckner's model was found most suitable and therefore recommended for estimating PWV for the location with range between 3.253 and 4.662 cm. The highest PWV occurred in June for Won and Leckner's models while for Smith's model it occurred in September; the lowest PWV occurred in January for all the evaluated models. The result showed that high values of dew point temperature (T_{dew}), PWV and relative humidity (RH) were observed during the raining season and low values in the dry season; this is an indication that the dew point temperature is a reflection of the PWV and RH. The dew point temperature is an opposite reflection of the virtual temperature ($T_{virtual}$), potential temperature ($T_{potential}$) and mean temperature (T_{mean}). The dew point temperature increases and decreases with mean temperature in the months from January to March and in July respectively for the location under investigation. The values of the dew point temperature indicated that the air is stable signifying no development of severe weather condition like thunderstorms. The maximum and minimum virtual temperature correction of 3.3246°C and 2.3371°C occurred in June and January respectively while for the dew point depression, it occurred in the months of January and September with 8.7514°C and 2.1094°C. The descriptive statistical analysis shows that the dew point temperature, potential temperature, mean temperature and virtual temperature correction data spread out more to the left of their mean value (negatively skewed), while the virtual temperature and dew point depression data spread out more to the right of their mean value (positively skewed). The dew point temperature and the virtual temperature correction data have positive kurtosis which indicates a relatively peaked distribution and possibility of a leptokurtic distribution while the virtual temperature, potential temperature, mean temperature and dew point depression data have negative kurtosis which indicates a relatively flat distribution and possibility of platykurtic distribution.

Keywords: Precipitable Water Vapour, Dew Point Temperature, Relative Humidity, Virtual Temperature, Potential Temperature and Mean Temperature

1. Introduction

Water vapor plays a vital role in climate change, hydrological processes, Earth's energy balance, and weather systems [1-3]. Water vapor is the most abundant greenhouse gas in the atmosphere, and it accounts for about 60% of the natural greenhouse effect [4]. As a result of this, the saturation vapor pressure is expected to increase as a response to rises in air temperature. Therefore, atmospheric water vapor provides a strong positive feedback for global warming as well as carbon (iv) oxide, ozone, methane, and other greenhouse gases [1, 5-9]. Thus, the processes on how water vapor changes in both the real atmosphere and climate models is significant, not only for a better understanding of water vapor feedback on global warming but also for the exploration of climate change [10].

Water vapor absorbs most solar radiation and is considered the most important green house gas in the atmosphere [11]. It can also lead to global warming as it is the major cause of the green house effect. It cycles continuously through the process of evaporation and condensation, transporting heat energy around the earth and between the surface and the atmosphere [12].

The quantity of liquid water that would be acquired if all the vapour in the atmosphere within the vertical column were compressed to the point of condensation is called PWV [13]. Generally, the standard methods for PWV measurement are radiosondes [14], ground-based microwave radiometers, LIDAR systems [15-16], LASER systems [17] and GPS satellites [18-22]. Nevertheless, each method has its own drawbacks. LIDAR measurements are costly [23]. Low spatial resolution restricts the use of space based instruments [23]. It is almost impossible to quantify an exact PWV trend from radiosonde PWV owning to limitations such as incomplete and inhomogeneous observations and sparse spatial distributions [7, 24]. Furthermore, numerous factors such as variation in instrumentation, uncontrollable balloons, upgrades to instruments, and temporal inhomogeneities sometimes cause spurious shifts in the radiosonde PWV time series [25].

The temperature at which the moisture/liquid water (water vapour) in the atmosphere evaporates at same rate at which it condenses is known as dew point temperature. Dew point temperature values are vital to meteorologists because it measures essentially the state of the atmosphere based on how much water vapor is present [26]. Similarly, dew point temperature offers a fairly direct sense of how comfortable or uncomfortable warm air is felt. Dew point provides us with an idea for forecasting the next day low temperatures, under certain conditions the lowest temperature tends to be close to the dew point at the time of maximum temperature the day before [27]. The values of dew point temperature aids in prognosticating the formation of fog or dew and in estimating rain, snow, dew, evapotranspiration, near surface humidity and other meteorological parameters. In addition, higher dew points through the troposphere (especially those above 60°C) can help to support more numerous and/or severe thunderstorms when other factors favor their formation. The importance of dew point temperature affects us in one way or the other especially when one recognizes this important factor, the amount of moisture in a gas, impacts much more than Heating, Ventilation and Cooling (HVAC) considerations. (i) It is an essential factor in convective heat transfer, combustion of fossil fuels and combustion engineering, drying of paper, cardboard, plastics, wood, tobacco, leather, printed goods, textiles and grain. (ii) It plays a key role in the efficient use of energy in many chemical manufacturing processes as well as the attainment of high product yield. (iii) The effect of moisture in gases also plays a very important role in corrosion phenomena which can result in damage and loss of not only unprotected metals, like iron and steel structural components, but also improperly treated or stored steel and other metal products [28].

The virtual temperature is the temperature that dry air would need to attain in order to have the same density as the moist air at the same pressure. Because moist air is less dense than dry air at the same temperature and pressure, the virtual temperature is always greater than the actual temperature. However, even for very warm and moist air, the virtual temperature exceeds the actual temperature by only a few degrees [29].

The potential temperature $T_{potential}$ of an air parcel is defined as the temperature that the parcel of air would have if it were expanded or compressed adiabatically from its existing pressure and temperature to a standard pressure p_0 (generally taken as 1000 hPa) [29].

The purpose of this study was to (i) compare three precipitable water vapour (PWV) models to ascertain their suitability for Owerri (ii) to estimate dew point temperature and to investigate its variation with the PWV, relative humidity, virtual temperature, potential temperature and mean temperature. (iii) Evaluation of virtual temperature correction and dew point depression along with descriptive statistical analysis.

2. Study Area

Figure 1 shows the study area under investigation. Imo is a state in Nigeria located in south eastern Nigeria. Owerri (Latitude 5.48°N, Longitude 7.00°E, and 91 m above sea level) is the capital city of Imo and one of the largest in the state. The State is bordered by Abia State on the East, River Niger and Delta State to the West, Anambra State on the North and Rivers State to the South. Based on the changes that occur as a result of rising surface temperature and rainfall, the area is likely vulnerable to the consequences of global warming [30]. Two seasons are identified, wet and dry seasons. The rainy season is from April to October while the dry season is from November to March. Double maxima, with the first maximum in June and the second in September also characterized the climate. There is therefore a "little dry season" in-between known as "August Break" brought about by the seasonal north and southward movement of the ITCZ

(Inter-Tropical Convergence Zone). An average annual temperature above 20°C (68.0°F) creates an annual relative humidity of 75%, with humidity reaching 90% in the rainy season [30]. The dry season experiences two months of Harmattan from late December to late February. January and March are the hottest months [30].

Imo state has three main political zones; this are, Okigwe (Imo North), Orlu (Imo West) and Owerri (Imo East). According to Okorie [31], the state has a population of about 3, 927, 563 with male, 1, 976, 471 and female 1, 951, 092. The state is blessed with natural resources which include, crude oil, natural gas, lead and zinc. Economically exploitable flora like the iroko, mahogany, obeche, bamboo, rubber tree and oil palm predominate [30].

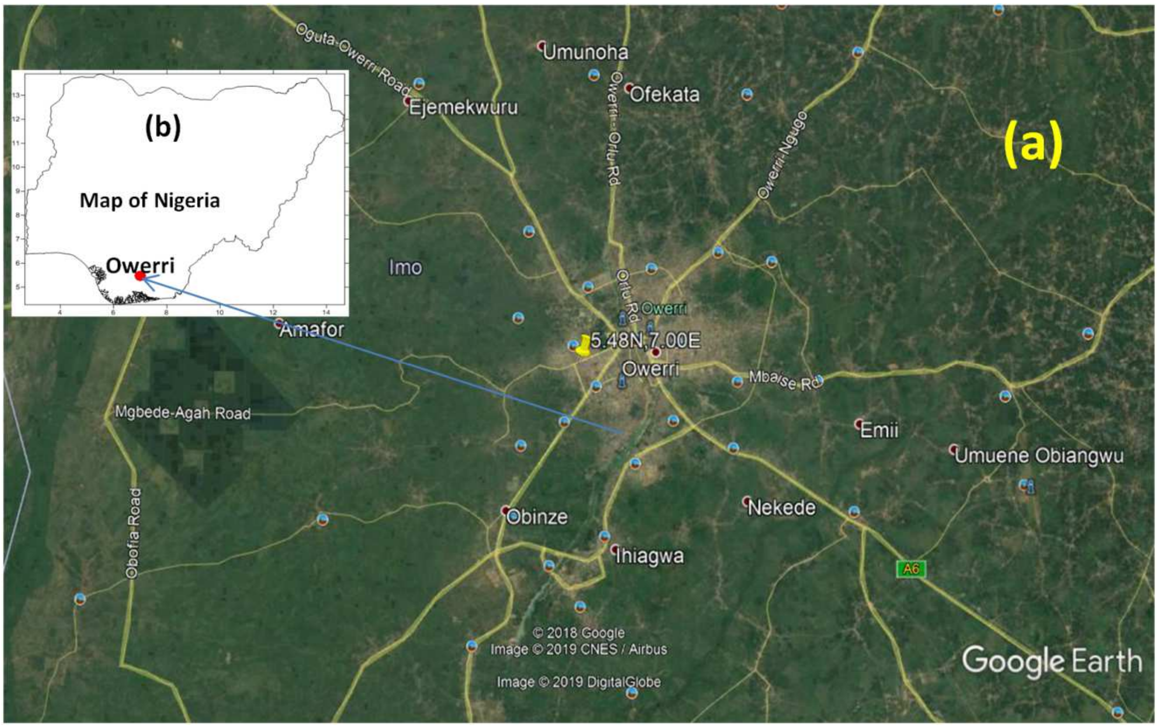

Figure 1. *Map of (a) Google map showing the study area (b) Map of Nigeria showing the study area.*

3. Methodology

The monthly average minimum temperature, maximum temperature and relative humidity meteorological data used in this study were obtained from the European Centre for Medium-Range Weather Forecasts (ECMWF) at 2m height for owerri, Imo state located in the South Eastern, Nigeria during the period of sixteen years (2000-2015).

Smith [32] developed a correlation between precipitable water and dew point temperature. The coefficients in this correlation vary with latitude and season. Atwater and Ball [33] simplified Smith [32] correlation to

$$w^{`} = \exp(0.07074\, T_{dew} + D) \quad (1)$$

where $w^{`}$ is in centimeters, T_{dew} is the station's dew-point temperature in degrees Celsius and $D = -0.02290$ from April to June and 0.02023 for the remaining months.

For all seasons, Won [34] has developed a simple correlation as follows

$$w^{`} = 0.1 \exp(2.2572 + 0.05454\, T_{dew}) \quad (2)$$

The precipitable water as obtained from Equations (1) and (2) applies to prevailing station pressure and temperature. However, the attenuation equations often require this quantity to be reduced to a datum of 1013.25 mbars pressure and 273 K temperature. Paltridge and Platt [35] suggest the following formula for reduction of $w^{`}$ to the datum conditions:

$$w = w^{`}\left(\frac{p}{1013.25}\right)^{3/4}\left(\frac{273}{T}\right)^{1/2} \quad (3)$$

where w is the reduced precipitable water in centimeters, p is station pressure in millibars, and T is the surface (dry-bulb) temperature in degrees Kelvin.

Leckner [36] has presented the following formula, which expresses precipitable water in terms of relative humidity:

$$w = \frac{0.493\, \varphi_r p_s}{T} \quad (4)$$

where φ_r is relative humidity in fractions of one, T is ambient temperature in degrees Kelvin and p_s is the partial pressure of water vapour in saturated air and is given by the semi empirical equation as

$$p_s = \exp(26.23 - \frac{5416}{T}) \quad (5)$$

The pressure and temperature correction is not necessary in equation (4) since it is already included in its numerical constant.

The dew point temperature (T_{dew}) was obtained using [37] as:

$$T_{dew} = T - \left[\frac{(100-RH)}{5}\right] \tag{6}$$

where T and RH are the mean temperature and relative humidity in degree Celsius and percentage respectively.

The Virtual temperature ($T_{virtual}$) was obtained using the expression [29] as

$$T_{virtual} = \frac{T}{1-\frac{e}{p}(1-\varepsilon)} \tag{7}$$

where e is water vapour pressure and ε is a constant given as $\varepsilon = 0.622$

The Potential temperature ($T_{potential}$) was obtained using the expression [29] as

$$T_{potential} = T_{mean}\left(\frac{p_0}{p}\right)^{R/c_p} \tag{8}$$

Equation (8) is called Poisson's equation, where p_0 is a standard pressure generally taken as 1000 hPa and $R/c_p = 0.286$.

The virtual temperature (T_{vc}) correction is given by [29] as.

$$T_{vc} = T_{virtual} - T_{mean} \tag{9}$$

The dew point depression ($T_{depression}$) is given by [29] as.

$$T_{depression} = T_{mean} - T_{dew} \tag{10}$$

In this paper, the skewness and kurtosis tests were studied. The skewness test (σ_k) measures the asymmetry of the parameters data around their mean value; it is a measure of symmetry, or more precisely, the lack of symmetry [38]. It gives information about the direction of variation of the dataset [38]. If $\sigma_k = 0$, the data have a Gaussian distribution (normal distribution), while $\sigma_k < 0$ indicates that the data are spread out more to the left of the mean value than to its right (negatively skewed), when $\sigma_k > 0$ signifies that data are spread out more to the right than to its left (positively skewed) [39].

The Kurtosis test (k_u) explains the shape of a random variable's probability distribution, that is it characterizes the relative peakedness or flatness of a distribution compared to the normal distribution [38]. It measures the degree of normality of each of the meteorological parameters under investigation [39]. For $k_u = 0$ the data have normal distribution, for $k_u > 0$ the data have positive kurtosis which connotes peaked distribution, that is, leptokurtic distribution (that is, too tall), when $k_u < 0$ the data have negative kurtosis which implies flat distribution, that is, platykurtic distribution (that is, too flat, or even concave if the value is large enough).

4. Results and Discussion

The result in figure 2 revealed that; the Smith's model increases from its minimum value of 3.436 cm in the month of January to March and slightly decreases in April and then increases to July and decreases with a dip downward in the month of August and then increases to its maximum value of 4.807 cm in the month of September and drop subsequently to December.

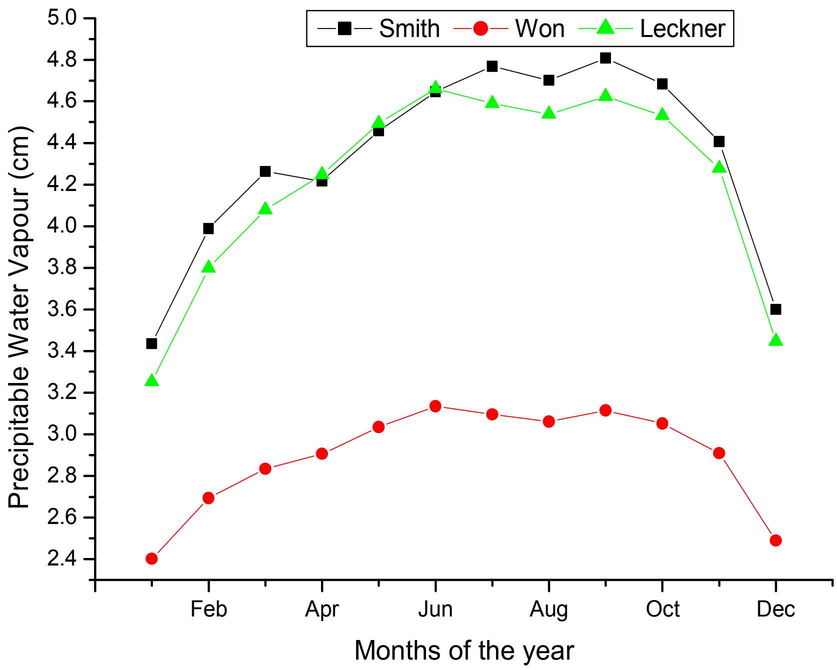

Figure 2. *Monthly variation of Precipitable Water Vapour Models at Owerri, Nigeria.*

The Won's model increases from its minimum value of 2.401 cm in the month of January and attained its maximum value of 3.135 cm in June and then decreases to August and slightly increases to September and drop subsequently to December.

The Leckner's model increases gradually from its minimum value of 3.253 cm in the month of January and attained its maximum value of 4.662 cm in the month of June and then decreases to August and slightly increases to September and drop subsequently to December.

The result of the Won's model showed that the precipitable water vapour are far away from the other models; however, the Leckner's model slightly overestimated the Smith's model in the months of April, May and June. The Leckner's precipitable water vapour model is found in between the two models and was reported most suitable model for estimating precipitable water vapour for the study area, since statistical test for validation was not carried out. The conclusion drawn from this as to which model is most suitable for PWV estimation is in conformity with the study analyzed in [40].

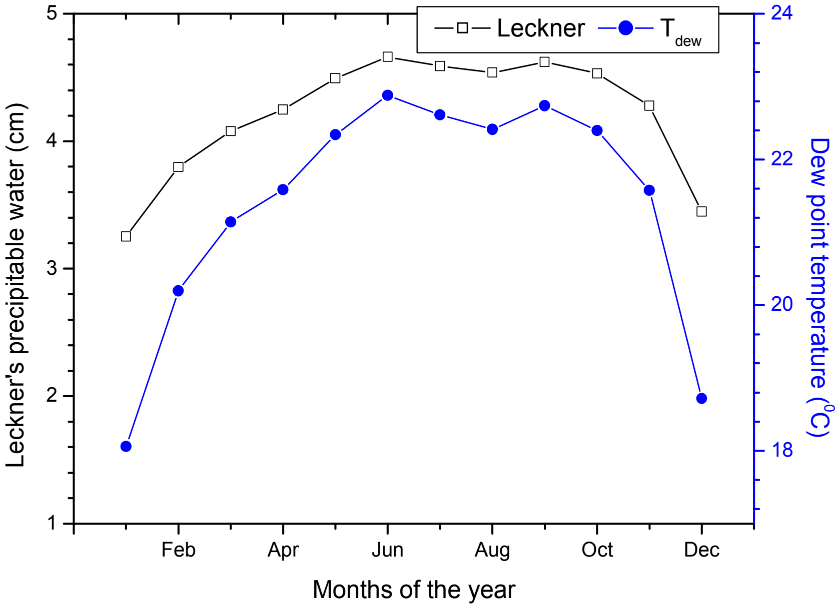

Figure 3. *Monthly variation of Dew Point Temperature with Precipitable Water Vapour at Owerri, Nigeria.*

Figure 3 shows the variation of dew point temperature with precipitable water vapour for the location under investigation. The dew point temperature and precipitable water vapour increases from their minimum value of 18.061°C and 3.253 cm in the month of January and attained their maximum value of 22.879°C and 4.662 cm in the month of June and decreases from June to August with a dip downward; though the dew point temperature is more conspicuous. The dew point temperature and precipitable water vapour increases to September and drop to December. The result indicated high and low values of dew point temperature and precipitable water vapour during the raining and dry seasons respectively. The result further showed that the dew point temperature is a reflection of the precipitable water vapour.

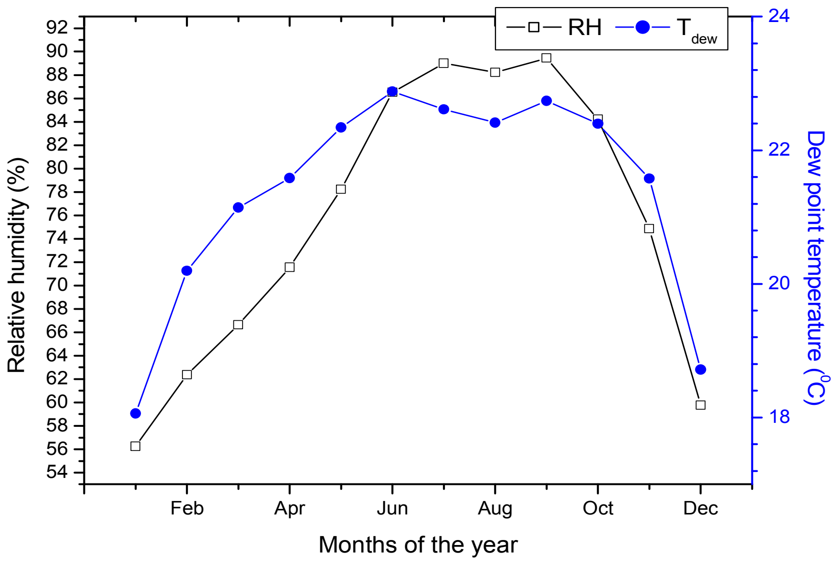

Figure 4. *Monthly variation of Dew Point Temperature with Relative Humidity at Owerri, Nigeria.*

Figure 4 shows the variation of dew point temperature with relative humidity for the location under investigation.

The relative humidity increases from its minimum value of 56.243% in the month of January to 89.002% in July and then decreases slightly in the month of August and increases to its maximum value of 89.453% in September and drop subsequently to December. The dew point temperature follows similar pattern of variation except that its minimum value of 18.061°C was observed in the month of January and maximum value of 22.879°C in the month of June; the decrease in the value of dew point temperature begins from July while for relative humidity is from August. High and low values of dew point temperature and relative humidity were observed during the raining and dry seasons respectively. The result of this study revealed that the dew point temperature is a reflection of relative humidity.

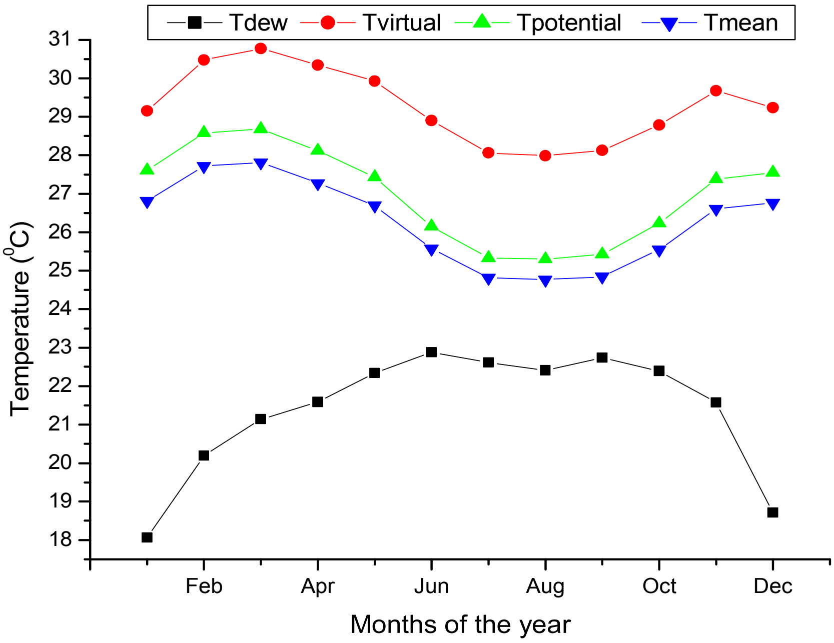

Figure 5. *Monthly variation of* T_{dew}, $T_{virtual}$, $T_{potential}$ *and* T_{mean} *for Owerri, Nigeria.*

Figure 5 shows the monthly variation of dew point temperature, virtual temperature, potential temperature and mean temperature for the location under investigation. The result revealed that the virtual temperature is greater than the dew point temperature, potential temperature and mean temperature while the dew point temperature has the lowest value. The potential temperature and mean temperature follows similar pattern of variation and the virtual temperature follows almost similar pattern of variation; the virtual temperature, potential temperature and mean temperature increases slightly from January to March and decreases from March to July and maintain almost a constant value from July to September and increases from September to December while the virtual temperature decreases slightly from November to December. On the other hand, the dew point temperature increases from it minimum value of 18.061°C in the month of January and attained its maximum value of 22.879°C in the month of June and decreases from June to August with a dip downward and then increases to September and drop to December. The result of this study showed high values of virtual temperature, potential temperature and mean temperature during the dry season and low values during the raining season while for the dew point temperature high values were recorded during the raining season and low values during the dry seasons; this shows that the dew point temperature is an opposite reflection of the virtual temperature, potential temperature and mean temperature. Considering the dew point temperature and the mean temperature; the dew point temperature increases with increase in mean temperature from January to March and decreases with decrease in mean temperature in the month of July for the location under investigation. The result indicated that the dew point temperature is always less than the mean/air temperature which implies that mean temperature cannot be lower than the dew point temperature; this helps meteorologists predict temperature lows in a weather forecast. The moderate values of the dew point temperature signifies the stability of air for the study area and less tendency of development of thunderstorms as very high dew point temperature can bring about severe weather condition.

Table 1. *Monthly average virtual temperature correction and dew point depression for Owerri, Nigeria.*

Month	T_{dew} (°C)	$T_{virtual}$ (°C)	$T_{potential}$ (°C)	T_{mean} (°C)	T_{vc} (°C)	$T_{depression}$ (°C)
JAN	18.0611	29.1496	27.6106	26.8125	2.3371	8.7514
FEB	20.196	30.4729	28.5771	27.7219	2.751	7.5259
MAR	21.1418	30.7715	28.6814	27.8125	2.959	6.6708
APR	21.5848	30.3427	28.1172	27.2719	3.0709	5.6871
MAY	22.3406	29.9304	27.4276	26.6969	3.2335	4.3563
JUN	22.8794	28.8996	26.1501	25.575	3.3246	2.6956

Month	T_{dew} (°C)	$T_{virtual}$ (°C)	$T_{potential}$ (°C)	T_{mean} (°C)	T_{vc} (°C)	$T_{depression}$ (°C)
JUL	22.6129	28.0658	25.3269	24.8125	3.2533	2.1996
AUG	22.4121	27.9845	25.2998	24.7688	3.2158	2.3566
SEP	22.7375	28.1267	25.4255	24.8469	3.2798	2.1094
OCT	22.3973	28.7847	26.2327	25.5500	3.2347	3.1528
NOV	21.5740	29.6792	27.3792	26.6031	3.0761	5.0291
DEC	18.7168	29.2391	27.5460	26.7625	2.4766	8.0458
Average	21.3878	29.2872	26.9812	26.2695	3.0177	4.8817

The maximum and minimum virtual temperature correction of 3.3246°C and 2.3371°C was obtained in the months of June and January with an average value of 3.0177°C. The maximum and minimum dew point depression of 8.7514°C and 2.1094°C was obtained in the months of January and September with an average value of 4.8817°C. The result shows that the maximum and minimum dew point depression and virtual temperature correction occurred in the month of January. The average dew point temperature, virtual temperature, potential temperature and mean temperature are 21.3878°C, 29.2872°C, 26.9812°C and 26.2695°C respectively for Owerri during the period under investigation.

Table 2. *Descriptive statistical analysis for the estimated parameters for Owerri, Nigeria.*

	Range	Minimum	Maximum	Sum	Skewness	Kurtosis
	Statistic	Statistic	Statistic	Statistic	Statistic	Statistic
T_{dew}	4.8183	18.061	22.879	278.04	-1.279	0.762
T_{vitual}	2.787	27.985	30.772	380.73	0.082	-1.041
$T_{potential}$	3.3816	25.300	28.681	350.76	-0.175	-1.262
T_{mean}	3.0437	24.769	27.813	341.50	-0.155	-1.240
T_{vc}	0.9875	2.3371	3.3246	39.23	-1.279	0.686
$T_{depression}$	6.642	2.1094	8.7514	63.462	0.326	-1.273

The results shown in Table 2 showed that the dew point temperature, potential temperature, mean temperature and virtual temperature correction data spread out more to the left of their mean value (negatively skewed), while the virtual temperature and dew point depression data spread out more to the right of their mean value (positively skewed). The virtual temperature, potential temperature, mean temperature and dew point depression data seem to have a quassi-Gaussian distribution. Skewness of exactly zero is quite not likely for real world data [38]. The dew point temperature and virtual temperature correction data are more divergent away from the normal distribution. It is clear from Table 2 that the dew point temperature and the virtual temperature correction data have positive kurtosis which indicates a relatively peaked distribution and possibility of a leptokurtic distribution. The virtual temperature, potential temperature, mean temperature and dew point depression data have negative kurtosis which indicates a relatively flat distribution and possibility of platykurtic distribution.

5. Conclusion

This study presents the distribution of monthly mean Precipitable water vapour (PWV) based on three models, the Smith; Won; and the Leckner's model using meteorological parameters of monthly mean temperature and relative humidity obtained from the European Centre for Medium-Range Weather Forecasts (ECMWF) at 2m height for Owerri, Imo state located in the South Eastern, Nigeria during the period of sixteen years (2000-2015). The distribution of PWV showed clear differences; the Smith (ranging from 3.436 to 4.807 cm); Won (ranging from 2.401 to 3.135 cm) and the Leckner's model (ranging from 3.253 to 3.135 cm). The highest PWV occurred in June for Won and Leckner's model while for Smith's model it occurred in September. The lowest PWV occurred in January for all the models. High values of virtual temperature, potential temperature and mean temperature were observed during the dry season and low values during the raining season while for the dew point temperature and RH, high and low values were observed during the raining and dry seasons respectively; this is an indication that the dew point temperature is an opposite reflection of virtual temperature, potential temperature and mean temperature. However, the dew point temperature is a reflection of the relative humidity. The values of the dew point temperatures indicated that the air is stable and less occurrences of thunderstorm; in view of these, this present study would help to guide against the episodes of climate induced environmental disaster like thunderstorm and can also enhance agricultural production in the study area. The maximum and minimum virtual temperature correction of 3.3246°C and 2.3371°C occurred in June and January while for the dew point depression it occurred in the months of January and September with 8.7514°C and 2.1094°C. The average dew point temperature, virtual temperature, potential temperature and mean temperature are 21.3878°C, 29.2872°C, 26.9812°C and 26.2695°C for Owerri during the period under study. The descriptive statistical analysis shows that the dew point temperature, potential temperature, mean temperature and virtual temperature correction data spread out more to the left of their mean value (negatively skewed), while the virtual temperature and dew point depression data spread out more to the right of their mean value (positively skewed). The dew point temperature and the virtual temperature correction data have positive kurtosis which indicates a relatively peaked distribution and possibility of a leptokurtic distribution while the virtual temperature, potential temperature, mean temperature and dew point depression data have negative kurtosis which indicates a relatively flat distribution and possibility of platykurtic distribution for the location under investigation.

Acknowledgements

The authors wish to thank the European Centre for Medium-Range Weather Forecasts (ECMWF) for providing all the necessary meteorological data used in this study. The contribution and suggestions of the anonymous reviewers is well appreciated.

References

[1] Held, I. M and Soden, B. J (2000). Water vapor feedback and global warming, Annual Review of Environment and Resources. vol. 25, pp. 441-475.

[2] Trenberth, K. E., Fasullo, J and Smith, L (2005). Trends and variability in column-integrated atmospheric water vapor. Climate Dynamics, vol. 24, no. 7-8, pp. 741-758.

[3] Wang, J., Carlson, D. J., Parsons, D. B et al (2003). Performance of operational radiosonde humidity sensors in direct comparison with a chilled mirror dew-point hygrometer and its climate implication. Geophysical Research Letters. vol. 30, no. 16.

[4] Wagner, T., Beirle, S., Grzegorski, M et al (2006). Global trends (1996-2003) of total column precipitable water observed by Global Ozone Monitoring Experiment (GOME) on ERS 2 and their relation to near-surface temperature. Journal of Geophysical Research: Atmospheres. vol. 111, no. 12, Article IDD12102.

[5] Dai, A (2006). Recent climatology, variability, and trends in global surface humidity," Journal of Climate. vol. 19, no. 15: pp. 3589- 3606.

[6] Dai, A., Wang, J., Thorne, P. W et al (2011). A new approach to homogenize daily radiosonde humidity data. Journal of Climate. vol. 24, no. 4: pp. 965-991.

[7] Zhao, T., Dai, A and Wang, J (2012). Trends in tropospheric humidity from 1970 to 2008 over china from a homogenized radiosonde dataset. Journal of Climate. vol. 25, no. 13: pp. 4549-4567.

[8] Mieruch, S., No¨el, S., Bovensmann, H et al (2008). Analysis of global water vapour trends from satellite measurements in the visible spectral range. Atmospheric Chemistry and Physics. vol. 8, no. 3, pp. 491-504.

[9] Zhang, L., Wu, L and Gan, B (2013). Modes and mechanisms of global water vapor variability over the twentieth century. Journal ofClimate. vol. 26, no. 15, pp. 5578-5593 USA.

[10] Peng, W., Tongchuan, X., Jiageng, D et al (2017). Trends and Variability in Precipitable Water Vapor throughout North China from 1979 to 2015. Hindawi Advances in Meteorology. Volume 2017, Article ID 7804823, PP 1-10.

[11] Kiehl, J. T and Trenberth, K. E (1997). Earth's Annual Global Mean Energy Budget. Bull Am Meteorol Soc. 78: 197-208.

[12] Adeyemi, B (2009). Empirical Formulations for Inter-Layer Precipitable Water Vapor in Nigeria. The Pacific Journal of Science and Technology. Volume 10, Number 2: Pp 35-45.

[13] Dupont, J. C., Haeffelin, M., Drobinski, P et al (2008). Parametric model to estimate clear-sky long wave irradiance at the surface on the basis of vertical distribution of humidity and temperature. J. Geophys. Res. 113, D07203. http://dx.doi.org/10.1029/2007JD009046

[14] Lanzante, J. R., Klein, S. A and Seidel, D. J (2003). Temporal homogenization of monthly radiosonde temperature data. Part II: Methodology. J. Climate 16: 224-240.

[15] Gerding, M., Christoph, R., Marion, M et al (2004). Tropospheric water vapour soundings by lidar at high Arctic latitudes. Atmos. Res. 71 (4), 289-302.

[16] Kuwahara, T., Mizuno, A., Nagahama, T et al (2008). Groundbased millimeter-wave observations of water vapor emission (183 GHz) at Atacama. Chile. Adv. Space Res. 42 (7): 1167-1171.

[17] Eng, R. S., Kelley, P. L., Mooradian, A et al (1973). Tunable laser measurements of water vapor transitions in the vicinity of 5 lm. Chem. Phys. Lett. 19 (15), 524-528.

[18] Bevis, M., Businger, S., Herring, T. A et al (1992). GPS meteorology. Remote sensing of atmospheric water vapour using the Global Positioning System. J. Geophys. Res. 97: 15784-15801.

[19] Hagemann, S., Bengtsson, L and Gendt, G (2003). On the determination of atmospheric water vapor from GPS measurements. J. Geophys. Res., 4678.

[20] Li, G., Kimura, F., Sato, T et al (2008). A composite analysis of diurnal cycle of GPS precipitable water vapor in central Japan during Calm Summer Days. Theoret. Appl. Climatol. 92 (1/2): 15.

[21] Stoew, B., Elgered, G., Johansson, J. M (2001). An assessment of estimates of integrated water vapor from ground-based GPS data. Meteorol. Atmos. Phys. 77, 99-107.

[22] Pramualsakdikul, S., Haas, R., Elgered, G et al (2007). Sensing of diurnal and semi diurnal variability in the water vapour content in the tropics using GPS measurements. Meteorol. Appl. 14, 403-412.

[23] Maghrabi, A and Al Dajani, H. M (2013). Estimation of precipitable water vapour using vapour pressure and air temperature in an arid region in central Saudi Arabia. Journal of the Association of Arab Universities for Basic and Applied Sciences. 14, 1-8.

[24] Dee, D. P., Uppala, S. M., Simmons, A. J et al (2011). The ERA-Interim reanalysis: configuration and performance of the data assimilation system. Quarterly Journal of the Royal Meteorological Society. vol. 137, no. 656, pp. 553-597.

[25] Easterling, D. R and Peterson, T. C (1995). A new method for detecting undocumented discontinuities in climatological time series. International Journal of Climatology. vol. 15, no. 4: pp. 369-377.

[26] Raymond, A. S (1991). College physics. Saunders College Publishing, Harrisonburg, Virginia.

[27] Kingsley, E. U., Samuel, O. A., Abiodun, I. C. A et al (2017). Approximation of the Dew Point Temperature Using a Cost Effective Weather Monitoring System. Physical Science International Journal. 14 (3): 1-6.

[28] Moss, M (2016). Capitol broadcasting company. Raleigh, North Carolina, USA; 2016.

[29] Wallace, J. M and Hobbs, P. V (2006). Atmospheric Science, An Introductory Survey, 2nd Edition, Elsevier, pp 66-82.

[30] Okorie, F. C., Okeke, I., Nnaji, A et al (2012). Evidence of Climate Variability in Imo State of Southeastern Nigeria. Journal of Earth Science and Engineering. 2 (2012) 544-553.

[31] Okorie, F. C (2010). Great Ogberuru in Its Contemporary Geography, Cape Publishers, Owerri, Nigeria.

[32] Smith, W (1966). Note on the relationship between total precipitable water and surface dew point. J. Appl. Meteorol. 5, 726-727.

[33] Atwater, M. A and Ball, J. T (1976). Comparisons of radiation computations using observed and estimated precipitable water. Appl. Meteorol. 15: 1319-1320.

[34] Won, T (1977). The simulation of hourly global radiation from hourly reported meteorological parameters Canadian Prairie Area. Conference, 3rd, Canadian Solar Energy Society Inc., Radiative Processes in Meteorology and Climatology. American Elsevier, New York.

[35] Paltridge, G. W and Platt, C. M. R (1976). Radiative Processes in Meteorology and Climatology. American Elsevier, New York, 1976.

[36] Leckner, B (1978). The spectral distribution of solar radiation at the earth's surface—elements of a model. Sol Energy 20 (2), 143-150.

[37] Lawrence, M. G (2005). The relationship between relative humidity and the dewpoint temperature in moist air: A simple conversion and applications. Bull. Amer. Meteor. Soc., 86, 225-233. doi: http;//dx.doi.org/10.1175/BAMS-86-2-225.

[38] Akpootu, D. O., Iliyasu, M. I., Mustapha, W et al (2017). The Influence of Meteorological Parameters on Atmospheric Visibility over Ikeja, Nigeria. Archives of Current Research International. 9 (3): 1-12. doi: 10.9734/ACRI/2017/36010.

[39] Hejase, H. A. N and Assi, A. H (2011). Time-Series Regression Model for Prediction of Monthly and Daily Average Global Solar Radiation in Al Ain City-UAE. Proceedings of the Global Conference on Global Warming held on 11-14 July, 2011, Lisbon, Portugal. Pp 1-11.

[40] Iqbal, M (1983). An Introduction to Solar Radiation. Academic Press, New York.

Journal of Water Resources and Ocean Science
2019; 8(3): 37-43
http://www.sciencepublishinggroup.com/j/wros
doi: 10.11648/j.wros.20190803.12
ISSN: 2328-7969 (Print); ISSN: 2328-7993 (Online)

Geoelectrical Investigation of Groundwater Potential, at Bosso Campus, Minna, Niger State, Nigeria

Aisha Alkali, Jamilu Shehu, Usman Defyan Alhassan, Kazeem Adeyinka Salako, Abdulwaheed Adewuyi Rafiu, Abbas Adebayo Adetona, Usman Usman Hussaini

Department of Geophysics, Federal University of Technology, Minna, Nigeria

Email address:
jameelshehu@futminna.edu.ng (J. Shehu)

To cite this article:
Aisha Alkali, Jamilu Shehu, Usman Defyan Alhassan, Kazeem Adeyinka Salako, Abdulwaheed Adewuyi Rafiu, Abbas Adebayo Adetona, Usman Usman Hussaini. Geoelectrical Investigation of Groundwater Potential, at Bosso Campus, Minna, Niger State, Nigeria. *Journal of Water Resources and Ocean Science*. Vol. 8, No. 3, 2019, pp. 37-43. doi: 10.11648/j.wros.20190803.12

Received: June 18, 2019; **Accepted**: July 10, 2019; **Published**: October 12, 2019

Abstract: Geoelectrical investigation of groundwater potential has been carried out at Bosso Staff Quarters Bosso campus, Federal university of Technology, Minna. The area is situated on latitude $9^0$38'55.8"N and $9^0$39'29.0"N and longitude $6^0$31'19.7"E and $6^0$31'46.7"E. the survey was carried out with the aim of delineating the potential area for groundwater development and depth to the groundwater within the study area. The Schlumbeger array was used to sound six profiles with a total of 36 Vertical Electrical Sounding (VES) points. The sounding interpretation results were used to generate geoelectric section. The corresponding geologic section were also generated which revealed the existence of three subsurface layers. These layers revealed the existence of three subsurface layers. These layers comprise the top soil, weathered/fractured basement and fresh basement. The results of this analysis are presented as curves of apparent resistivity versus depth, from the digitalized curves obtained from the IP2WIN software, sulfur 11 was used to generates iso-resistivity map at different depth. The analysis of results shows that the area is not appropriate for borehole drilling.

Keywords: Geoelectric, Vertical Electrical Sounding, Groundwater Potential and Subsurface Layer

1. Introduction

Nigeria is considered to be abundantly blessed with water resources. However, there is temporal and spatial variation in water availability, the north with low precipitation of only about 500 mm in the northeastern region, and the south with low precipitation of over 4,000 mm in the southeast [5] According to the United Nations Development Programme, meaningful progress in water supply is fundamental environmental sustainable development. Food production as well as other socio-economic activities depends on availability of water [13]. Water has been a very important factor in settlement development in the country where it usually serves as human settlement boundaries [6]. Geophysical techniques together with geological, structural and hydrogeological mapping have shown a positive synergy. Understanding structures is the key to interpreting crustal movements that have shaped the present terrain. Structures also indicate potential sites for locating water, oil and gas reserved by characterizing both the underlying subsurface geometry of rock units and the amount of crustal deformation experienced by the rock body [10].

Nearly all the water in the ground comes from precipitation that has infiltrated into the earth. Observations have shown that a good deal of surplus rainfall runs off over the surface of the ground while the other part of it infiltrates underground and becomes the groundwater responsible for the springs, lakes and wells [9].

Groundwater can be used for agricultural, municipal and industrial works. Groundwater is also widely used as a source for drinking supply and irrigation [4] About 53% of all population relies on groundwater as a source of drinking water. Most human requires about 2.5 litres of water everyday which justifies that the average amount of water used each day domestically by every person is around 190 litres [6].

Vertical Electrical Sounding (VES) is a geoelectrical method used to measure vertical alterations of electrical resistivity. The method has been recognised to be more suitable for a hydrogeological survey of the sedimentary basin [8]. Vertical Electrical Sounding has proven very popular with groundwater prospecting and engineering investigations due to simplicity of the techniques [1].

2. Geology of the Area

The study area is the school's field, adjacent the school's clinic, Bosso campus of Federal University of Technology Minna, Niger State which is part of Bosso local government in the city of Minna, Niger State, Nigeria. Bosso and its environs is the centre and major metropolitan of Minna the capital city of Niger State and has a land mass area of about 884 hectares [12].

The area investigated is part of the north-central Basement Complex of Nigeria which is composed of three lithological units, migmatite-gneiss complex, low grade schist belts and the older granite. Geological mapping revealed that the study area is underlain by granites, schist and gneiss with granites occupying greater portion of the area [7]. The structural mapping carried out in the area shows two principal joint directions along NE-SW and NW-SE. The river Chanchaga at the southern part of the study area which flows eastwards is structurally controlled.

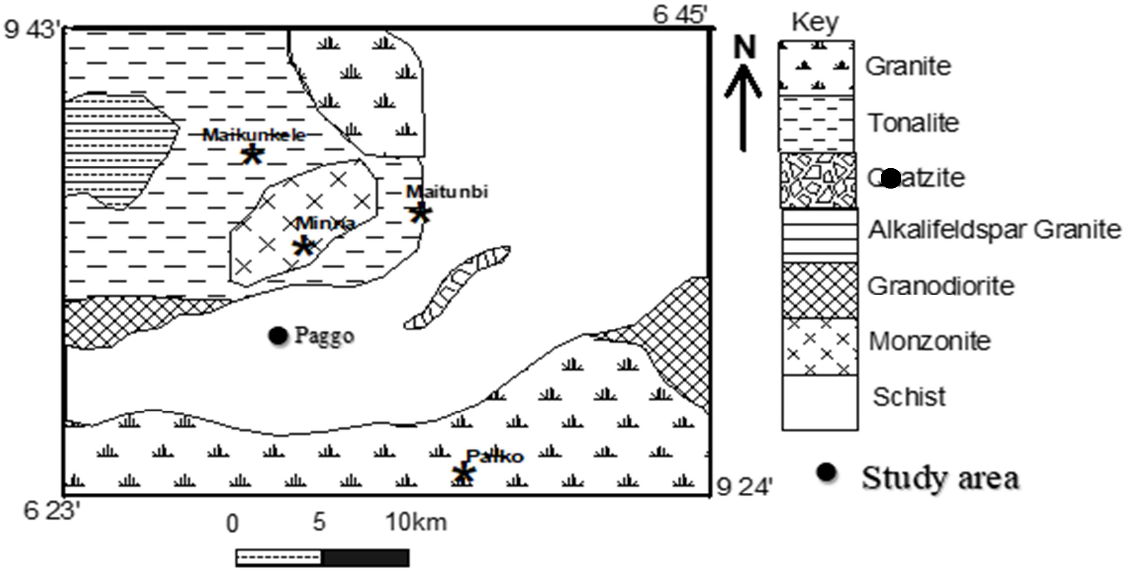

Figure 1. *Geological Map of Minna [5].*

3. Materials and Methods

The data was acquired with the Geotron G41Terrameter, Global Positioning System (GPS) for taking accurate coordinate of the VES point and elevations, Metal Electrodes, Measuring Tape, Labelled Tag (used in locating station position), Hammer (used in driving the electrodes into the ground). The Schlumberger array was adopted. The electrode spread of AB/2 was varied from 1 to a maximum of 100 m. Sounding data were presented as sounding curves, by plotting apparent resistivity against AB/2. The electrical resistances obtained were multiplied by the corresponding geometric factor (k) for each electrode separation to obtain the apparent resistivity. The IPI2win software was then used to obtain the n-layer model curve for the Schlumberger sounding curves. This software automatically interprets the Schlumberger sounding curves. The plotted curves reveal the number of layers, thickness, depth and the average resistivity for each VES points automatically.

Resistivity measurements are to ascertain the level of water saturation and conductivity variation. This is because water has low resistance, and this makes the passage of electric current suitable. Water is being released and resistivity is increased by the increasing compaction of soil or rock units [14] expressed that the measurements of water are connected with the variability of depths with respect to the current and potential electrodes separation used in the survey, and can be illustrated in terms of lithological and geohydrological model of the subsurface [11].

Ground resistivity is measured by passing an electric current through the ground using two current electrodes and measuring the resultant potential using two or more potential electrodes. The depth of investigation is often given as a function of the electrode spacing. That is to say that the greater the spacing between the outer current electrodes, the deeper the electrical currents will flow in the Earth, thus the greater the depth of exploration. Therefore, the depth of investigation is normally 20% to 40% of the current electrode spacing depending on the structure of the Earth resistivity. Ohms law is generally used to calculate the resistance which is then multiplied by a geometric factor (usually denoted as K) to calculate resistivity [14] as shown in equations (1) and (3).

Assuming an electrically conductive body lends itself to the description of a one-dimensional body (like a wire), the relationship between the current and potential distribution could be described by Ohm's law as:

$$V=IR \tag{1}$$

where V = the potential difference (in volts), I= current (in Amperes) and R = resistance (in ohms)

The resistance is therefore given by:

$$R = \frac{V}{I} = \rho\left(\frac{L}{A}\right) \quad (2)$$

For an area, A ($2\pi r^2$), equation (2) could be rewritten in terms of voltage, V as;

$$V = \frac{\rho I}{2\pi r} \quad (3)$$

Considering an electrode pair with current I at the first electrode, and –I at the second electrode the potential at any point is given by the algebraic sum of the individual contributions. Hence,

$$V = V_{c1} + V_{c2} = \rho I\left(\frac{1}{2\pi r_{c1}} - \frac{1}{2\pi r_{c2}}\right) = \frac{\rho I}{2\pi}\left(\frac{1}{r_{c1}} - \frac{1}{r_{c2}}\right) \quad (4)$$

where r_{c1} and r_{c2} = distances from the point between electrodes C1 and C2 respectively [16].

For the potential electrodes, P1 and P2 the potential is given as:

$$V = V_{P1} - V_{P2} = \frac{\rho I}{2\pi}\left(\frac{1}{C1P1} - \frac{1}{C2P1} + \frac{1}{C2P2} - \frac{1}{C1P2}\right) \quad (5)$$

where V_{P1} and V_{P2} = potentials at P_1 and P_2

C1P1 = distance between C_1 and P_1

C1P2= distance between C_1 and P_2

When we represent

$$\frac{1}{2\pi}\left(\frac{1}{AM} - \frac{1}{BM} + \frac{1}{BN} - \frac{1}{AN}\right) = \frac{1}{K} \quad (6)$$

Equation (5) becomes

$$V = \frac{\rho I}{K} \quad (7)$$

From which resistivity is calculated i.e.:

$$\rho = \frac{KV}{I} = R_{app}K \quad (8)$$

where ρ = resistivity (in ohm m), R_{app} = apparent resistance (in ohm) and K = geometric factor (in m).

The geometric factor, K varies for different electrode configurations. According to [15], the geometric factor, K for the Wenner array is 2πa. That of the Schlumberger array is given as;

$$\frac{\pi}{a}\left[\left(\frac{s}{a}\right)^2 - \left(\frac{a}{2}\right)^2\right] \quad (9)$$

and the dipole-dipole array is given as

$$\pi n(n+1)(n+2)a$$

where a = electrode spacing

s = distance

n = dipole length factor.

4. Results and Discussions

4.1. Criteria for Selecting Drilling Points

Geoelectric methods for groundwater prospecting depend on the correlation of subsurface electrical properties. Resistivity profiling was conducted and selected points within low resistive zones were selected for vertical electrical sounding. It is important to note that low resistive zones may not all be potential groundwater areas. Depths with high resistivities may have hard consolidated material like granites, boulders or a dike–like structure, whereas low resistivities could be an indication of zones of fractured/weathered rocks or clays [2].

4.2. Data Interpretation

Table 1. *Data Interpretation for Profile A.*

Profile Name	VES station	LITHOLOGY	Layers	Res. (Ωm)	Thickness (m)	Depth (m)
A	A1	Top soil	1	5.03	2.05	2.05
		Fractured basement	2	51.8	48.2	50.3
		Fresh basement	3	5.03	∞	∞
	A2	Top soil	1	1.91	1.99	1.99
		Clay / Clayey sand	2	50.3	18.7	20.7
		Fresh Basement	3	2.07	∞	∞
	A3	Top Soil	1	1.91	1.99	1.99
		Clay/Clayey sand	2	50.3	17.9	19.9
		Fresh Basement	3	1.99	∞	∞
	A4	Top soil	1	1.92	2.12	2.12
		Fractured Basement	2	52.2	17.1	19.2
		Fresh Basement	3	2.02	∞	∞
	A5	Top Soil	1	10.03	2.11	2.11
		Clayey sand	2	100	46.7	48.8
		Fresh basement	3	10.03	∞	∞
	A6	Clay	1	193	2.05	2.05
		Fractured Basement	2	3115	46.7	48.8
		Fresh Basement	3	103	∞	∞

Table 2. *Data Interpretation for Profile B.*

Profile Name	VES station	LITHOLOGY	Layers	Res. (Ωm)	Thickness (m)	Depth (m)
B	B1	Top soil	1	2.74	1.99	1.99
		Fractured basement	2	161	18.5	20.5
		Fresh basement	3	1.99	∞	∞
	B2	Top soil	1	0.671	2.05	2.05
		Clay / Clayey sand	2	20.5	18.4	20.5
		Fresh Basement	3	0.658	∞	∞
	B3	Top Soil	1	58.3	2.02	2.02
		Clay/Clayey sand	2	367	45.7	47.7
		Fresh Basement	3	63.1	∞	∞
	B4	Top soil	1	0.412	1.91	1.91
		Fractured Basement	2	19.9	18.8	20.7
		Fresh Basement	3	0.524	∞	∞
	B5	Top Soil	1	5.78	1.99	1.99
		Clayey sand	2	205	18.5	20.5
		Fresh basement	3	6.78	∞	∞
	B6	Clay	1	36.4	1.98	1.98
		Fractured Basement	2	626	47.6	49.6
		Fresh Basement	3	36.7	∞	∞

Table 3. *Data Interpretation for Profile C.*

Profile Name	VES station	LITHOLOGY	Layers	Res. (Ωm)	Thickness (m)	Depth (m)
C	C1	Top soil	1	32.3	1.99	1.99
		Fractured basement	2	1989	17.9	19.9
		Fresh basement	3	35.1	∞	∞
	C2	Top soil	1	74	2.05	2.05
		Clay / Clayey sand	2	1432	17.3	19.3
		Fresh Basement	3	81.1	∞	∞
	C3	Top Soil	1	1.3	2.05	2.05
		Clay/Clayey sand	2	20.5	48.2	50.3
		Fresh Basement	3	1.39	∞	∞
	C4	Top soil	1	6.74	2.07	2.07
		Fractured Basement	2	191	46.3	48.3
		Fresh Basement	3	6.68	∞	∞
	C5	Top Soil	1	68.24	2.015	2.015
		Clayey sand	2	444.1	48.61	50.62
		Fresh basement	3	67	∞	∞
	C6	Clay	1	0.711	2.02	2.02
		Fractured Basement	2	21.2	19.2	21.2
		Fresh Basement	3	0.741	∞	∞

Table 4. *Data Interpretation for Profile D.*

Profile Name	VES station	LITHOLOGY	Layers	Res. (Ωm)	Thickness (m)	Depth (m)
D	D1	Top soil	1	0.0427	2.02	2.02
		Fractured basement	2	0.496	47.6	49.6
		Fresh basement	3	0.0449	∞	∞
	D2	Top soil	1	1.49	2.12	2.12
		Clay / Clayey sand	2	49.6	18	20.2
		Fresh Basement	3	1.57	∞	∞
	D3	Top Soil	1	5.05	2.05	2.05
		Clay/Clayey sand	2	199	18.4	20.5
		Fresh Basement	3	4.88	∞	∞
	D4	Top soil	1	2.57	1.99	1.99
		Fractured Basement	2	50.3	46.3	48.3
		Fresh Basement	3	2.53	∞	∞
	D5	Top Soil	1	12.4	2.05	2.05
		Clayey sand	2	205	48.2	50.3
		Fresh basement	3	12	∞	∞
	D6	Clay	1	2.23	1.91	1.91
		Fractured Basement	2	48.3	48.4	50.3
		Fresh Basement	3	2.15	∞	∞

Table 5. *Data Interpretation for Profile E.*

Profile Name	VES station	LITHOLOGY	Layers	Res. (Ω*m*)	Thickness (m)	Depth (m)
E	E1	Top soil	1	0.946	1.99	1.99
		Fractured basement	2	50.3	17.1	19.1
		Fresh basement	3	0.96	∞	∞
	E2	Top soil	1	0.0163	2.02	2.02
		Clay / Clayey sand	2	0.496	17.2	19.2
		Fresh Basement	3	0.0173	∞	∞
	E3	Top Soil	1	3.37	2.02	2.02
		Clay/Clayey sand	2	47.2	47.6	49.6
		Fresh Basement	3	3.32	∞	∞
	E4	Top soil	1	0.371	2.12	2.12
		Fractured Basement	2	21.2	18	20.2
		Fresh Basement	3	0.386	∞	∞
	E5	Top Soil	1	10.1	1.99	1.99
		Clayey sand	2	96	48.3	50.3
		Fresh basement	3	10	∞	∞
	E6	Clay	1	2.17	1.99	1.99
		Fractured Basement	2	50.3	48.3	50.3
		Fresh Basement	3	2.07	∞	∞

Table 6. *Data Interpretation for Profile F.*

Profile Name	VES station	LITHOLOGY	Layers	Res. (Ω*m*)	Thickness (m)	Depth (m)
F	F1	Top soil	1	0.114	2.12	2.12
		Fractured basement	2	10	7.88	10
		Fresh basement	3	0.116	∞	∞
	F2	Top soil	1	1.27	1.99	1.99
		Clay / Clayey sand	2	48.8	17.9	19.9
		Fresh Basement	3	1.2	∞	∞
	F3	Top Soil	1	0.873	2.07	2.07
		Clay/Clayey sand	2	19.9	17.8	19.9
		Fresh Basement	3	0.886	∞	∞
	F4	Top soil	1	1.83	1.99	1.99
		Fractured Basement	2	51.8	46.8	48.8
		Fresh Basement	3	1.99	∞	∞
	F5	Top Soil	1	0.0451	2.07	2.07
		Clayey sand	2	10	7.34	9.41
		Fresh basement	3	0.0455	∞	∞
	F6	Clay	1	0.0286	1.92	1.92
		Fractured Basement	2	362	3.3	5.22
		Fresh Basement	3	548	∞	∞

4.3. Iso-resistivity Map

Through the computer aided software called Surfer, the iso resistivity map of an area is defined. The map helps to show the resistivity/conductivity variation with depth through the entire study area horizontal cross-section slicing. It also helps to delineate the lateral variation of the sub-surface geology of an area. These maps include the resistivity map of the topmost layer, 5m, 10m, 15m e.t.c depth variation [3].

4.3.1 Iso-resistivity Map at the Surface

The iso-resistivity contour map at the surface was contoured at 50 Ωm interval as shown in figure 2. The map shows a spatial variation of the resistivity of the topmost layer, which could be used to compare with the surface features like stream and exposed outcrops. The low range value region represents the loose earth material. The loose earth materials includes top soil, sandstone, clayey sand, humus e.t.c. The fractured or fairly weathered basement was found with resistivity value range between 330 Ωm and 860 Ωm. The fresh basement rock of very high resistivity value of 1160 Ωm was found prominent.

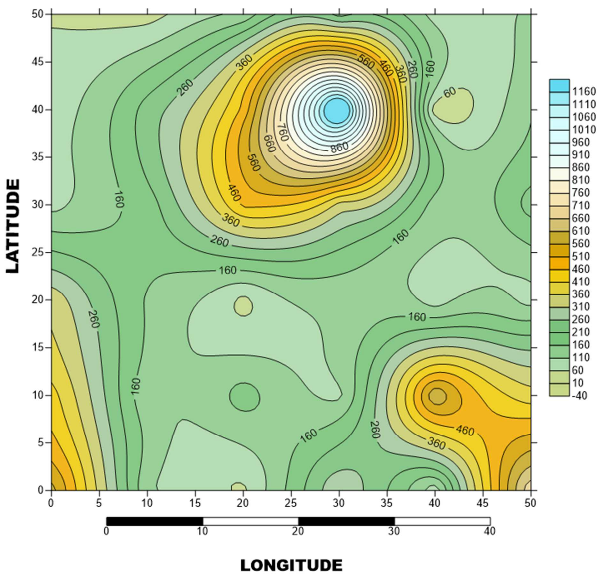

Figure 2. *Iso-resistivity Map of the top soil.*

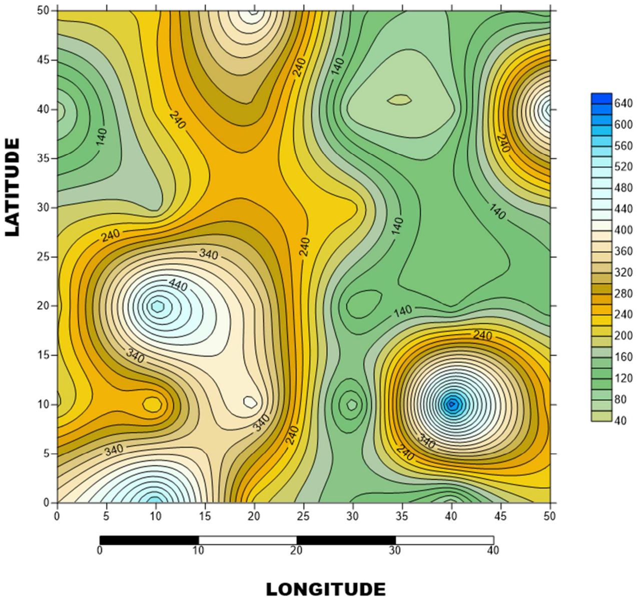

Figure 3. Iso-resistivity Map at the 5m depth.

4.3.2. Iso-resistivity Map at 5 m

The figure 3 shows a 20 Ωm interval contoured iso-resistivity map at 5m depth The low range value region represents the loose earth material. The loose earth materials signifies the top soil variation range with a resistivity value of 140 Ωm. Also the highest resistivity value recorded within the fresh basement is 640 Ωm.

4.3.3. Iso-resistivity Map at 10 m

The figure 4 shows a 500 Ωm interval contoured iso-resistivity map at 10m depth. The depth range signifies no saturated (water) horizons within the subsurface. The fresh basement rock of very high resistivity value was recorded within the resistivity range of 5500 Ωm - 8000 Ωm.

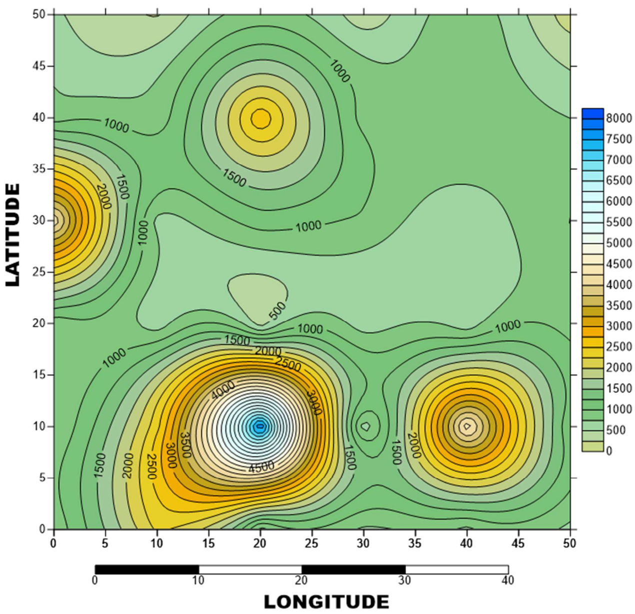

Figure 4. Iso resistivity at 10m depth.

5. Conclusion

In this study, the groundwater potential was undertaken using vertical electrical soundings (VES). The curve type are simple three-layer types. The computer assisted sounding interpretation revealed subsurface sequence composing top-soil with limited hydrologic significance. The interpretation of the sounding results revealed that most of the profiles were underlain by an overburden thickness ranging from 12 to 16m. Moderately weathered material ranging from less than one meter to several meters in thickness separate the overburden from the underlying fractured bedrock and the hard bedrock. The bedrock may be associated with fractures in some of the communities and these resulted in relatively lower resistivities. Therefore the study area may be considered very poor for groundwater development.

6. Recommendations

The researcher observes that profiling at a constant depth of 60 m is a limitation on the study because prospective water-bearing zones could occur beyond this depth; hence further studies could be done to explore more boreholes in the district.

The electromagnetic method using Omega-M 2000 resistivity meter could also be used to locate resistivity anomaly zones that have the potential to store groundwater.

Resistivity method used for the project was efficient and reliable as the success rate was 64%. Finally, further work to determine groundwater infiltration and consequent pollution from various minerals such as Iron, Magnesium and human activities should be done to ensure safety of consumers.

References

[1] Abiola O., P. A. Enikanselu and M. I. Oladapo (2009). Groundwater potential and aquifer protective capacity of overburden units in Ado-Ekiti, southwestern Nigeria *International Journal of Physical Sciences, 4 (3), 120-132*.

[2] Abdullahi N. K, Iheakanwa, A (2013). Groundwater Detection in Basement Complex of North- western Nigeria using 2D Electrical Resistivity and OffsetWenner Techniques, *International Journal of Science and Technology, 2 (7)*.

[3] Alhassan, D. U, Mohammed I. N, Bature. M, Kimpa, M. I, and Mohammed, A. (2015): Electrical Resistivity Survey For ground Water at Eye Zheba Village, Off Bida - Minna Road. *Journal of Applied Geology and Geophysics* (IOSR-JAGG) India, (3), 49-53.

[4] Alile, O. M., Ujuanbi, O. and Evbuomwan, I. A., 2011. Geoelectric investigation of groundwater in Obaretin Iyanomon locality, Edo state, Nigeria. *Journal of Geology and Mining Research*, *3* (1), pp. 13-20.

[5] Alabi, A. A., 2011. Geology and Environmental Impact Assessment and Benefit of Granitic Rocks of Minna area, Northwestern Nigeria. *Ethiopian Journal of Environmental Studies and Management*, 4: 39-45.

[6] Amadi, A. N., Olasehinde, P. I., Okosun, E. A. and Yisa, J., 2010. Assessment of the water quality index of Otamiri and Oramiriukwa Rivers. *Physics International*, *1* (2), pp. 116-123.

[7] Anomohanran, O., 2015. Hydrogeophysical investigation of aquifer properties and lithological strata in Abraka, Nigeria. *Journal of African Earth Sciences*, *102*, pp. 247-253.

[8] Iserhien-Emekeme, R. E., Atakpo, E. A., Emekeme, O. L. and Anomohanran, O., 2004. Geoelectric survey for groundwater in Agbede Etsako West LGA, Edo State. *Adv. Nat. Applied Sci. Res*, *2*, pp. 65-72.

[9] Oseji, J. O., Asokhia, M. B. and Okolie, E. C., 2006. Determination of groundwater potential in obiaruku and environs using surface geoelectric sounding. *Environmentalist*, *26* (4), pp. 301-308.

[10] Muchiri L. Ambusso W., Githiri J. & Cherop H.. (2016). Geophysical Investigation and Characterization of Groundwater Aquifers In Kangonde Area, Machakos County In Kenya Using Electrical Resistivity Method. *IOSR Journal of Applied Geology and Geophysics, 4 (2), 23-35*.

[11] Muturi N. Esther K. Maurice O. & Githiri J. G. (2014), Application of integrated geophysical techniques for groundwater potential evaluation in hard rock basement: mutito fault zone, Kenya, *International Journal of Current. Trend, 2 (1), 18-28.*

[12] Osinowo, O. O. Akanji, A. O. & Akinmosin A. (2011). Integrated geophysical and Geotechnical investigation of the failed portion of a road in basement complex Terrain, Southwest Nigeria. *Materials and Geoenvironment,* 58 (2), 143–162.

[13] Ozegin, K. O. Oseghale A. Okolie E. C. & Ujuanbi O. (2011). Integration of very low frequency electromagnetic (vlf-em) and electrical resistivity methods in mapping subsurface geologic structures favourable to road failures. *International Journal of Water Resources and Environmental Engineering*. 3 (6), 126-131.

[14] Plummer, C. C., McGeary, D. and Carlson, D. H., 1991. *Physical geology* (No. QE28. 2 P58 2005). Wm. C. Brown.

[15] Robinson, M. and Ward, R., 1990. *Principles of hydrology*. McGraw-Hill.

[16] Telford, W. M. Geldart, L. P. Sherrif, R. E. & Keys D. A. (1976). Applied Geophysics. Cambridge University press, London.

Call for Papers

Journal of Water Resources and Ocean Science (WROS)

http://www.sciencepublishinggroup.com/j/wros

Journal of Water Resources and Ocean Science (WROS) is an international journal whose aim is to achieve the advancement and dissemination of information in the field of water resources and ocean science. The journal is committed to the publication of original research articles, reviews and notes on all fields of water resources and oceanography including physical oceanography, biological oceanography/marine biology, chemical oceanography/marine chemistry, geological oceanography/marine geology, and marine pollution. *WROS* aims to promote rapid communication and dialogue among researchers, scientists, and engineers working in the areas of water resources and ocean science.

Subject Coverage

The topics related to this journal include but are not limited to:

- Surface and subsurface hydrology
- Modeling fluid flow
- Water economics
- Water education
- Chemical oceanography
- Marine pollution
- Hydrodynamics and hydrometeorology
- Mathematical and stochastic analysis
- Eco-hydrology
- Physical oceanography
- Geological oceanography geology
- Multiphase transport phenomena
- Watershed planning and management
- Water quality
- Biological oceanography

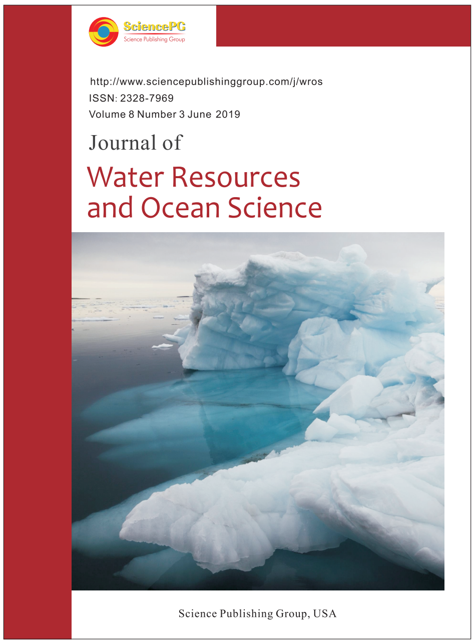

Notes for Intending Authors

Publishing your research in a Science Publishing Group journal is simple and efficient. Please use online submission system: http://www.sciencepublishinggroup.com/login

Only the following word processor file formats are acceptable for the manuscript document for all of Science Publishing Group journals: •Microsoft word 2000/2003(doc) •Microsoft word 2007/2010(docx)

Website and Email

http://www.sciencepublishinggroup.com/j/wros

Email: service@sciencepublishinggroup.com

Editorial Board

ISSN: 2328-7969 (Print), 2328-7993 (Online)

Science Publishing Group (SciencePG), an open access publisher with experienced and eminent reviewers and editorial board members, is mainly attaching importance to developing journals, books and conferences which have owned unique characters respectively. Here is the website of SciencePG: http://www.sciencepublishinggroup.com

ISSN: 2328-7969

9 772328 796002 03